Journal of Power Sources 266 (2014) 481–487

Contents lists available at ScienceDirect

Journal of Power Sources

journal homepage: www.elsevier.com/locate/jpowsour

# Effect of carbon material on Pd catalyst for formic acid electrooxidation reaction

Jinfa Chang [a], Songtao Li [c], Ligang Feng [b, *], Xiujuan Qin [a], Guangjie Shao [a, *]

[a] State Key Laboratory of Metastable Materials Science and Technology, Hebei Province Key Laboratory of Applied Chemistry, Yanshan University, Qinhuangdao 066004, PR China
[b] Institute of Chemical Sciences and Engineering, Ecole Polytechnique Fédérale de Lausanne (EPFL), ISIC-LSCI, BCH 3314, Lausanne 1015, Switzerland
[c] Institute of Mathematics, Jilin University, Changchun 130012, PR China

## HIGHLIGHTS

- Effect of carbon on palladium for formic acid oxidation was investigated.
- New active sites formed by the interaction of palladium and carbon.
- Carbon materials decrease charge transfer resistance.
- Mechanism of formic acid oxidation changed due to the presence of carbon.

## ARTICLE INFO

*Article history:*
Received 23 December 2013
Received in revised form
17 April 2014
Accepted 7 May 2014
Available online 21 May 2014

*Keywords:*
Formic acid electrooxidation
Pd catalyst
Carbon
Fuel cell

## ABSTRACT

Effect of several usually used carbon materials on Pd catalyst for formic acid electrooxidation reaction is studied by physical characterization and electrochemical measurements. New active sites are formed due to the Pd and carbon interaction which is confirmed by the XPS measurements, and electrochemical impedance spectroscopy confirms that the presence of the carbon material reduced the charge transfer resistance. Further, an improved fuel cell performance is observed when integrating the carbon-modified Pd catalyst in to a direct formic acid fuel cell. The results reveal that the carbon material is not only used as support, but also involves the new active sites formation.



## 1. Introduction

Formic acid electrooxidation has received great attention due to the development of the direct formic acid fuel cells, which are quite competitive in the aspect of actual fuel energy density [1–3]. It is well known that the research on electrocatalyst for formic acid electrooxidation is crucial for the development of formic acid fuel cells. Nowadays, in order to decrease the noble metal loading and the system cost, supported catalyst has been widely employed in the fuel cell technology [4,5]. Generally speaking, the main pathway is loading the noble metals (such as Pt or Pd) on the support by electrodeposition or chemical reduction of the precursor [6,7].

The carbon-supported catalyst has superior performance for formic acid electrooxidation because carbon is cheap and conductive support for efficient current collection from the catalyst layer. Moreover, the porous structure and good electrical conductivity of carbon support can provide good pathway for electrons and ions transfer during electrochemical reactions [7,8]. In addition to electrical conductivity and surface area, especially the hydrophobicity, porosity and corrosion resistance are more important factors in the choice of a good catalyst support. Based on these considerations, carbon is the best catalyst support material for the low temperature fuel cells. Carbon black and activated carbon have been extensively used as catalyst support [2,9,10]; moreover, a number of new carbon materials with various mesostructures and nanostructures as support have been reported [11–14]. It can be seen, a lot of carbon materials have been used as support to increase the catalytic performance; however, we didn't notice the research about the effect of carbon materials on Pd catalyst for

* Corresponding authors. Fax: +49 21 693 9305, +41 86 335 8061569.
*E-mail addresses:* ligang.feng@epfl.ch, fenglg11@gmail.com (L. Feng), shaogj@ysu.edu.cn (G. Shao).

http://dx.doi.org/10.1016/j.jpowsour.2014.05.043
0378-7753/

formic acid electrooxidation. Is the carbon only used as support? Is there any other effect of carbon on the active sites formation for formic acid oxidation? With these questions, we studied the effect of some typically used carbon materials on Pd catalyst performance for formic acid electrooxidation. In order to do the controllable experiments, we employ the physical mixed commercial Pd black and carbon materials for the comparative study as it can avoid the effect of synthesis methods, conditions, particle size and so on. The composite catalysts were studied for formic acid electrooxidation by the electrochemical methods of cyclic voltammograms (CV), Linear sweep voltammograms (LSV), chronoamperometry (CA), electrochemical impedance spectroscopy (EIS) as well as tested in a direct formic acid fuel cell, and the results displayed that both the catalytic activity and the stability of Pd catalyst for formic acid electrooxidation were enhanced after adding the carbon material, and the mechanism for the formic acid electrooxidation was changed due to the newly formed active sites. Because there are no obvious changes on the Pd particle size, the promotion effect should be attributed to the newly formed active sites originating from the interaction of Pd and carbon.

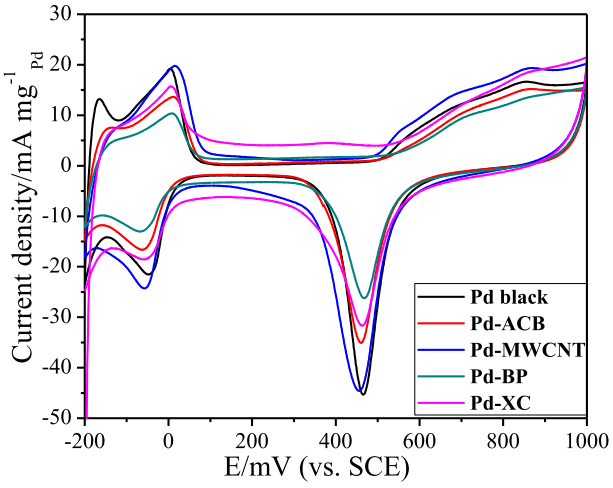


**Fig. 1.** CV curves of different catalysts in 0.5 M $H_2SO_4$ solution.

## 2. Experimental

### 2.1. Materials and reagents

The commercial Pd black (520810-5G, 50 $m^2$ $g^{-1}$) and formic acid (≥95%, F0507-1L) were purchased from Aldrich Chemical Co. (USA). The Vulcan carbon powder XC-72 (XC) and black pearls 2000 (BP) were purchased from Cabot Co. (USA). Acetylene carbon black (≥99.9%, 50% compressed, ACB) was purchased from J & K Technology Co., Ltd. (China). Multi-walled carbon nanotubes (≥97%, 5–15 μm in length, MWCNT) was purchased from Shenzhen Nanotech Port Co., Ltd., (China). Nafion solution (5%) was purchased from Dupont Co. (USA). The sulfuric acid (≥95%) and ethanol (≥99.7%) was purchased from Beijing Chemical Co. (China). All the chemicals were of analytical grade and used as received without any purification. Ultrapure water (resistivity: $\rho \geq 18$ MΩ $cm^{-1}$) was used to prepare the solutions.

### 2.2. Working electrode preparation

5 mg commercial Pd black and 20 mg MWCNT were ground into fine powders using a mortar and pestle with 30 min. After that, the solid mixture was added into the solution of 4750 μL ethanol and 250 μL Nafion ionomer, followed by ultrasonically to form a uniform catalyst ink, it was denoted as Pd–MWCNT. The catalyst inks for Pd–ACB, Pd–BP and Pd–XC were prepared using the same procedure to that of Pd–MWCNT except that MWCNT was substituted by ACB, BP and XC. The preparation method of the catalyst for commercial Pd black without adding any carbon material was the same to above method.

The glassy carbon electrode with 4 mm diameter was used as working electrode, and polished with alumina slurry of 0.5 and 0.03 μm successively. 5 μL of the as-prepared catalyst ink was pipetted and dropped on a mirror-finished glassy carbon electrode, and then it was dried at room temperature for 30 min. A Pt foil was used as the counter reference electrode and a saturated calomel electrode ($Hg/HgCl_2$, SCE) was used as reference electrode. All potentials were referenced to SCE.

### 2.3. Electrochemical measurements

All the electrochemical measurements were performed with an EG & G PARC potentiostat/galvanostat (Model 273A Princeton Applied Research Co., USA) and a conventional three-compartment electrochemical cell. All electrochemical measurements were carried out in a 0.5 M $H_2SO_4$ solution with or without 0.5 M HCOOH deaerated by pure $N_2$ for at least 20 min prior to any measurements. For the electrooxidation of formic acid, the scan potential range was from −200 mV to 1000 mV. The CO stripping voltammograms were measured in a 0.5 M $H_2SO_4$ solution, CO was purged into the 0.5 M $H_2SO_4$ solution for 15 min to allow the complete adsorption of CO onto the catalyst when the potential of working electrode was kept at 200 mV, and excess CO in the electrolyte was purged out with $N_2$ for 30 min. All scanning rates were 50 mV $s^{-1}$ and the measurements were carried out at room temperature, and the stable results were recorded. The EIS was recorded at the frequency range from 100 kHz to 0.1 Hz with 10 points per decade. The amplitude of the sinusoidal potential signal was 5 mV. The obtained impedance data were analyzed and fitted with ZsimpWin computer program.

### 2.4. Physical characterization

The size and morphology of the catalyst particles were measured by transmission electron microscope (TEM) operating at 200 kV (Philips TECNAI G2), the chemical valence of Pd was tested by X-ray photoelectron spectroscopy (XPS) measurements with Al $K_\alpha$ radiation source (Kratos XSAM-800 spectrometer) and The Pd 3d signals were collected and analyzed with deconvolution of the spectra using XPS Peak software.

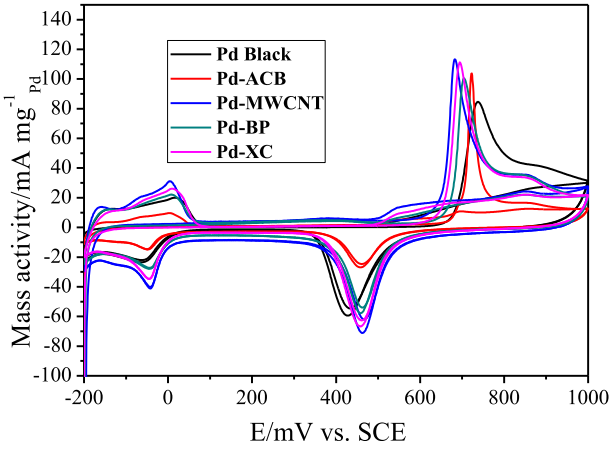


**Fig. 2.** The CO stripping curves of different catalysts in 0.5 M $H_2SO_4$ solution.

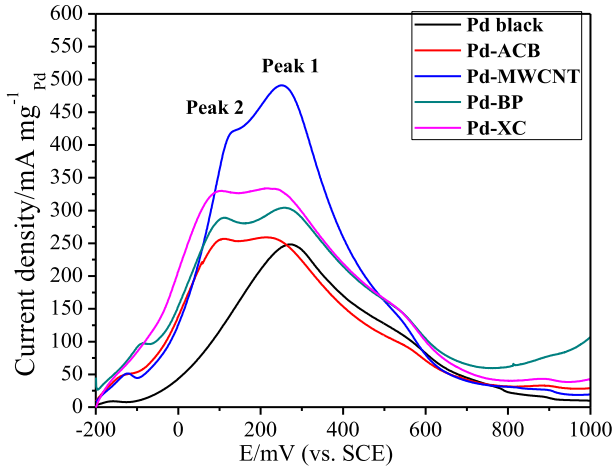


**Fig. 3.** LSV curves of different catalysts in 0.5 M $H_2SO_4$ solution containing 0.5 M HCOOH.

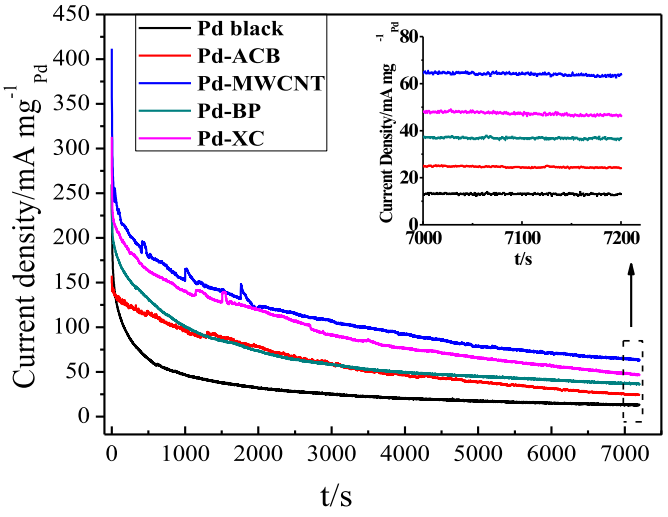


**Fig. 4.** CA curves of different catalysts in 0.5 M $H_2SO_4$ solution containing 0.5 M HCOOH at 0.2 V for 7200 s, inset is the steady CA curves between 7000 and 7200 s.

### 2.5. Membrane electrode assembly preparation

Nafion 117 (DuPont) was used as the proton exchange membranes and the pre-treatment of the Nafion membrane was accomplished by successively treating it in a 5 wt.% $H_2O_2$ solution at 80 °C, distilled water at 80 °C, 8 wt.% $H_2SO_4$ solution at 80 °C and then in distilled water at 80 °C again, for 30 min each step. Prior to the fabrication of hot-pressed Membrane electrode assemblies (MEA) and catalyst-coated membrane, a carbon cloth was used as Gas diffusion layer for current collector and it also assists in water management.

MEA with a 3 * 3 $cm^2$ active cell area was fabricated using a 'direct paint' technique applied to the catalyst layer. Pt black (27 $m^2$ $g^{-1}$, Johnson Matthey, USA) were used as catalyst in the cathode. The catalyst ink mixed by the catalyst, ultrapure water, isopropyl alcohol and 5 wt.% Nafion ionomer solution was sprayed onto the diffusion layer to fabricate the catalyst layers. Anode 'catalyst inks' were directly painted onto either side of a Nafion® 117 membrane. For all MEAs in this study, the cathode consisted of unsupported platinum black nanoparticles at a standard loading of 4 mg $cm^{-2}$ and the anode catalyst loading of the Pd was 2 mg $cm^{-2}$. The anode consisted of Pd black or Pd–C catalysts. A carbon cloth diffusion layer (E-TeK) was placed on top of both the cathode and anode catalyst layers. Both sides of the cathode carbon cloth were Teflon® coated for water management. A single cell test fixture consisted of machined graphite flow fields with direct liquid feeds and gold plated copper plates to avoid corrosion (Fuel Cell Technologies Inc.). Hot-pressing was conducted at 140 °C and 10 MPa for 90 s.

### 2.6. Single cell assembly and measurement

Five different anode catalysts were investigated in this study: (I) 18 mg commercial Pd black, (II) 18 mg Pd black and 72 mg acetylene carbon black, (III) 18 mg Pd black and 72 mg multi-walled carbon nanotubes, (IV) 18 mg Pd black and 72 mg black pearls 2000. (V) 18 mg Pd black and 72 mg Vulcan carbon powder XC-72.

The MEA was fitted between two stainless steel plates in a punctual flow bed. The polarization curves were obtained using a Fuel Cell Test System (Arbin Instrument Corp.) under the operation conditions of 60 °C. High purity $O_2$ (99.99%) is applied as the oxidant at 500 mL $min^{-1}$ as the cathode atmosphere and 3 M formic acid as the reactant feed on the anode side at 200 mL $min^{-1}$. Both two sides are under ambient pressure.

## 3. Results and discussion

### 3.1. Electrochemical analysis

Fig. 1 shows the CVs of different catalysts in 0.5 M $H_2SO_4$ solution. It is evident that all catalysts showed well defined hydrogen adsorption/desorption ($H_{ad}$) peaks and the redox peaks of Pd. All these features are typical for Pd in $H_2SO_4$ solution and agree well with the reported data in the literature [15,16]. Obviously, after adding the carbon material into the Pd black, the peak area for hydrogen oxidation was decreased, it could be due to the coverage up of the active sites by carbon material partly. Moreover, it can be seen that the peak area for the hydrogen desorption of the Pd black with different carbon materials was close, but lower than that of the pure Pd black except for the MWCNT one.

The peak potential of the adsorbed CO is commonly used as a tool to compare the anti-poisoning ability. Fig. 2 shows the CO stripping curves for different catalysts in 0.5 M $H_2SO_4$ solution. Typically, the peak potential of $CO_{ad}$ oxidation for Pd–MWCNT catalyst is ca. 682.44 mV, which is shifted about 55 mV to a lower potential than Pd black catalyst (ca. 737.60 mV). The peak potential of $CO_{ad}$ oxidation for Pd–ACB, Pd–BP and Pd–XC is 722.53, 704.41 and 694.56 mV, respectively. It is evident that the oxidation peak potential for $CO_{ad}$ oxidation of all Pd–C catalysts is shifted

**Table 1**
The peak current density and the corresponding peak potential for formic acid electrooxidation of the different catalysts in 0.5 M $H_2SO_4$ solution containing 0.5 M HCOOH.

| Sample | Pd black | Pd–ACB | | Pd–MWCNT | | Pd–BP | | Pd–XC | |
|---|---|---|---|---|---|---|---|---|---|
| | Peak 1 | Peak 1 | Peak 2 | Peak 1 | Peak 2 | Peak 1 | Peak 2 | Peak 1 | Peak 2 |
| Peak current density (mA $mg^{-1}_{Pd}$) | 247.9 | 256.8 | 259.0 | 419.6 | 491.0 | 288.8 | 304.1 | 392.9 | 333.9 |
| Peak potential (mV) | 269.7 | 109.8 | 217.8 | 129.7 | 251.8 | 112.9 | 259.8 | 104.9 | 217.8 |

negatively compared to Pd black, indicating that addition of carbon is helpful for weakening the adsorption strength of CO on Pd.

Fig. 3 shows the CV curves for different catalysts in 0.5 M $H_2SO_4$ solution containing 0.5 M HCOOH. It can be observed that the peak current density of pure Pd black electrode is 247.9 mA $mg^{-1}_{Pd}$ and the corresponding potential locates at ca. 269.7 mV. However, when the carbon material is added into the Pd black, it is interesting that two obvious peaks for formic acid oxidation were observed. One peak (named Peak 1) is very close to that of pure Pd black, it could be attributed to the role of intrinsic active sites similar to the Pd black; the other peak (named peak 2) is more negative than the peak of pure Pd black, it could be attributed to the role of new active sites produced by the interaction between the Pd and carbon materials. It should be pointed out that Peak 2 for Pd black may be present but it is not obvious; hence we didn't discuss it here. It can be seen from Fig. 3 that the Peak 1 for all carbon modified Pd black catalyst was negatively shifted compared with the pure Pd black catalyst, which indicated that formic acid oxidation reaction became much easier. Moreover, the peak potential (ca. 0.1 V) of peak 2 formed by the new active sites is ca. 150 mV which is more negative compared with the main Peak 1 formed by Pd intrinsic active sites indicating that the newly formed active sites are much active than the intrinsic active sites. This is consistent with the literature in which for the carbon supported Pd catalyst prepared with other methods, the peak potential of formic acid oxidation is also negatively shifted compared with that for pure Pd black catalyst [17,18]. Compared with the Pd/C catalysts prepared by chemical method [17,18], usually only one peak is observed resulting from the more active sites formed by the interaction between Pd and carbon material [15,19,20] and the potential is around 0.2 V which may be the compromise of the two peaks observed here. The peak current density and the corresponding peak potential for formic acid electrooxidation of the studied catalysts are listed in Table 1. It is evident that the carbon modified Pd black catalyst showed enhanced activity for formic acid oxidation; for example, Pd–MWCNT catalyst has the largest peak current density (491.0 mA $mg^{-1}_{Pd}$), and most negative peak potentials (Peak 1 at 251.8 mV and peak 2 at 125.2 mV). Besides, the current density of Peak 1 for all Pd black catalyst modified by carbon is much larger than that of pure Pd black should be due to the improvement of the dispersion for Pd nanoparticles and good conductivity; for the obvious Peak 2 observed for all the Pd black catalyst modified by carbon should be attributed to the newly produced active sites from the interaction of Pd and carbon.

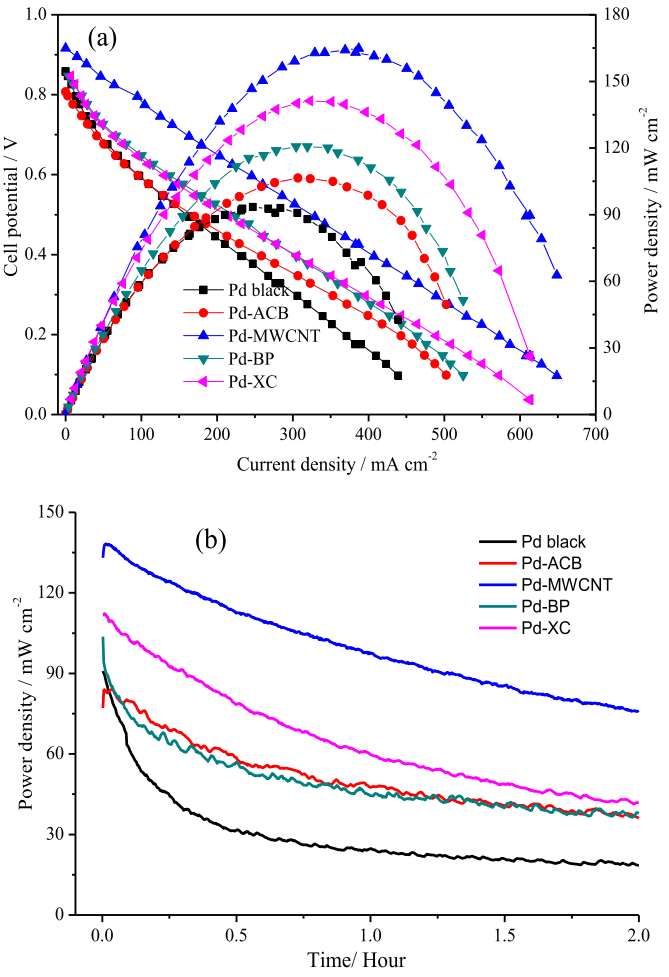


**Fig. 5.** Steady-state polarization, power–density curves (a) and discharge curves at 0.35 V (b) of the DFAFCs using Pd black, Pd–ACB, Pd–MWCNT, PD–BP and Pd–XC catalyst as anodes with formic acid (3 M) at 60 °C. The flow rate of formic acid was 200 mL $min^{-1}$ and the flow rate of $O_2$ was 500 mL $min^{-1}$.

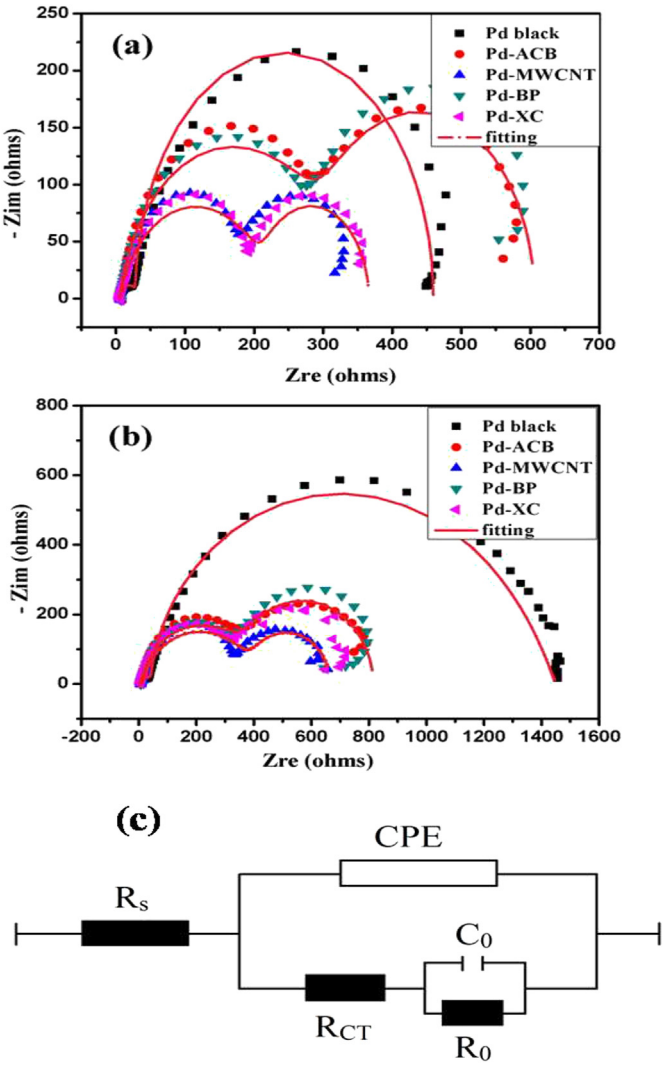


**Fig. 6.** EIS for different catalysts modified electrode in 0.5 M $H_2SO_4$ solution containing 0.5 M HCOOH at 0.2 V. (a) impedance patterns before 7200 s CA test and (b) impedance patterns after 7200 s CA test (solid pink lines are fitting curves); (c) represent the equivalent circuit. (For interpretation of the references to color in this figure legend, the reader is referred to the web version of this article.)

**Table 2**
EIS fitting parameters from equivalent circuits for different catalyst samples.

| | Sample | Error range | Pd black | Pd–ACB | Pd–MWCNT | Pd–BP | Pd–XC |
|---|---|---|---|---|---|---|---|
| Before CA | $R_S$ ($\Omega$ cm$^{-2}$) | ±0.001 | 5.977 | 5.732 | 5.867 | 5.580 | 5.238 |
| | CPE, $Y_0$ (S s$^{-n}$ cm$^{-2}$) | ±0.1E-6 | 150.0E-6 | 246.7E-6 | 342.0E-6 | 276.2E-6 | 171.6E-6 |
| | $n$ ($0 < n < 1$) | ±0.0002 | 1 | 0.8799 | 0.7526 | 0.8772 | 0.8080 |
| | $R_{CT}$ ($\Omega$ cm$^{-2}$) | ±0.1 | 229.2 | 205.0 | 150.8 | 320.8 | 218.3 |
| | $C_0$ (F cm$^{-2}$) | ±0.02E-5 | 2.10E-5 | 74.31E-5 | 255.1E-5 | 73.61E-5 | 39.67E-5 |
| | $R_0$ ($\Omega$ cm$^{-2}$) | ±0.2 | 428.5 | 123.9 | 23.4 | 280.5 | 143.1 |
| | Chi squared | – | 9.098E-3 | 6.008E-3 | 3.080E-3 | 8.425E-3 | 3.938E-3 |
| After CA | $R_S$ ($\Omega$ cm$^{-2}$) | ±0.001 | 6.588 | 5.936 | 5.923 | 5.615 | 6.076 |
| | CPE, $Y_0$ (S s$^{-n}$ cm$^{-2}$) | ±0.1E-6 | 36.6E-6 | 154.6E-6 | 278.4E-6 | 184.4E-6 | 173.6E-6 |
| | $n$ ($0 < n < 1$) | ±0.0002 | 0.9824 | 0.8675 | 0.7319 | 0.8686 | 0.8045 |
| | $R_{CT}$ ($\Omega$ cm$^{-2}$) | ±0.01 | 574.40 | 461.00 | 223.52 | 408.30 | 408.40 |
| | $C_0$ (F cm$^{-2}$) | ±0.02E-5 | 1.19E-5 | 450.10E-5 | 463.90E-5 | 284.8E-5 | 715.3E-5 |
| | $R_0$ ($\Omega$ cm$^{-2}$) | ±0.2 | 1386.0 | 355.5 | 72.1 | 402.4 | 252.3 |
| | Chi squared | – | 6.381E-3 | 5.357E-3 | 6.562E-3 | 7.931E-3 | 1.121E-3 |

The stability of the catalyst for formic acid oxidation was studied by CA and shown in Fig. 4. It is evident that the stability of the carbon modified Pd black catalyst is largely improved. For example, according to the inset in Fig. 4, the stable current density of Pd–MWCNT electrode (64.3 mA mg$^{-1}_{Pd}$) is 4.0 times larger than that of pure Pd black electrode (12.8 mA mg$^{-1}_{Pd}$); and the current of the Pd–XC (47.3 mA mg$^{-1}_{Pd}$), Pd–BP (36.4 mA mg$^{-1}_{Pd}$) and the Pd–ACB electrode (24.2 mA mg$^{-1}_{Pd}$) is ca. 2.7, 1.8 and 0.9 times larger than that of pure Pd black electrode. On the other hand, only 7.1% of the initial current density (take the current of 10 s) at the pure Pd black catalyst remained after 7200 s, while it is 22.3%, 20.5%, 17.8% and 13.8% for Pd–MWCNT, Pd–XC, Pd–BP Pd–ACB catalyst respectively, confirming a better electrocatalytic stability according to the references [21,22]. This result indicated an improved catalytic stability with the presence of carbon.

In order to further evaluate the performances of carbon-modified Pd catalyst as anode catalyst in a real fuel cell operation, the five different catalysts were integrated into the anode of a homemade direct formic acid fuel cell. The steady-state polarization, power–density curves and discharge curves of the studied catalysts were compared in Fig. 5. It can be seen from Fig. 5(a) that the maximum power density of Pd black, Pd–ACB, Pd–MWCNT, Pd–BP and PD–XC is 92.8, 106.2, 120.1, 142.14 and 163.6 mW cm$^{-2}$, respectively. Compared with the Pd black, Pd catalyst modified by carbon really increased the activity. Moreover, it can be seen from Fig. 5(b) that the discharge stability of all the modified Pd catalysts is largely improved compared with Pd black catalyst at 0.35 V. The above results are consistent with those results obtained from the CV and CA tests. However, it should be pointed out that the performance improvements was also limited due to the increased thickness of MEA by the addition of carbon material which could affect the mass transfer during formic acid oxidation process.

EIS is a powerful technique to characterize the electrode surface which has been widely employed to study the kinetics of electrochemical reaction [23,24] and was used to reveal the mechanism of electrooxidation of formic acid in the present work. Generally, a semicircle appeared in the intermediate frequency region

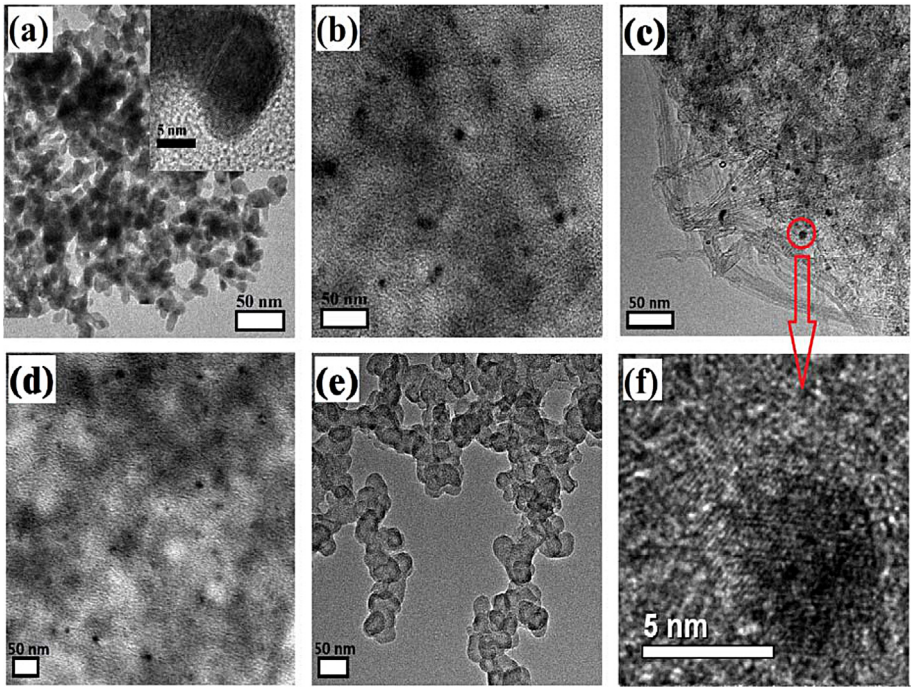


**Fig. 7.** TEM image for Pd black, inset is HRTEM images (a), Pd–ACB (b), Pd–MWCNT (c), Pd–BP (d), Pd–XC (e) and HRTEM image for Pd–MWCNT (f).

corresponds to the charge transfer resistance. Here, in order to know the changes of the catalyst, the impedance was done at 0.2 V before and after the CA tests as shown in Fig. 6(a) and (b). It is interesting that when the carbon material added into the Pd black a different impedance behavior is observed; namely, there is only one arc in the 1st quadrant for pure Pd black electrode, while there are two-stage arc for Pd–ACB, Pd–BP, Pd–XC and Pd–MWCNT electrode which may be explained by the two different active sites. For pure Pd black electrode, the impedance data in Nyquist plot shows a clockwise mode as the applied frequency decreases. Such a kind of EIS pattern is commonly observed [25,26]. Fig. 6(c) represents the equivalent circuit for different impedances and the corresponding fitting parameters were listed in Table 2. The fitting curves (solid pink lines) (in the web version) for the electrodes were shown in the Nyquist plot in Fig. 6(a) and (b), all of which agree well with the experimental data. Here, $R_s$ represents the solution resistance, $R_{CT}$ represents the charge transfer resistance, CPE (constant-phase element) is the double layer capacitance, $C_0$ and $R_0$ represent the capacitance and resistance of the electrooxidation of adsorbed intermediates [27]. It can be seen from Table 2 that the $R_{CT}$ derived from the carbon modified Pd black electrode is remarkably smaller than that of the Pd black electrode. Since charge transfer resistance is one of the main parameters to evaluate the inherent rate of the charge transfer step of an electrode reaction, the smaller $R_{CT}$ indicates that the electron-transfer kinetics for formic acid oxidation at the carbon modified Pd black electrode is much fast than the Pd black electrode. Furthermore, it can be seen that after the CA test, the $R_{CT}$ and $R_0$ were increased compared with those before CA test. This was caused by the intermediate products adsorbed on the catalyst surface. It also can be seen from Table 2 that $C_0$ derived from Pd–ACB, Pd–MWCNT, Pd–BP and Pd–XC is remarkably larger than pure Pd black electrode, while $R_0$ derived from carbon modified Pd black electrode is remarkably smaller than that of Pd black electrode, indicating that intermediates was easily oxidized after adding carbon material into the pure Pd black, which is consistent with the CV results that more formic acid was oxidized. According to Brug and Hirschorn's work [28–30], the impedance associated with a simple Faradaic reaction without diffusion can be expressed in terms of a CPE as

$$Z_{(\omega)} = R_S + \frac{R_{CT}}{1 + (j\omega)^n Q R_{CT}}$$

The CPE parameters $n$ and $Q$ are independent of frequency. When $n = 1$, $Q$ has units of a capacitance, i.e., μF cm$^{-2}$, and represents the capacity of the interface. When $n < 1$, the system shows behavior that has been attributed to surface heterogeneity or to continuously distributed time constants for charge-transfer reactions [31–33]. That means, for the pure Pd black electrode, there was only one time constant, while there was two time constants on Pd–ACB, Pd–MWCNT, Pd–BP and Pd–XC catalyst or the surface heterogeneity was enhanced. By comparing the simulated results among various catalysts, larger CPE and smaller $n$ values were found for the carbon modified Pd black electrode, corresponding to highly available surface area for electrochemical reactions and the diffusion of ions on the surface is easy.

### 3.2. Physical characterization

The TEM micrographs for different catalysts are presented in Fig. 7. Fig. 7(a) shows a typical micrograph of commercial Pd black, and the inset was a HRTEM micrograph for Pd black. The particle size of Pd black was approximately 10 nm, which is consistent with previous study [2] Fig. 7(b)–(e) were TEM micrographs for Pd–ACB, Pd–MWCNT, Pd–BP and Pd–XC, the corresponding average particle size of Pd was around 10 nm. It's obvious that the particle size of Pd on different carbon substrates was similar to that of pure Pd black. Hence, the enhanced electrocatalytic activity and stability cannot be attributed to the effect of Pd particle size.

The electronic structure change of Pd for all the catalysts was determined by XPS. As shown in Fig. 8, the Pd 3d peaks of each sample were deconvolved into two components, that is, $3d_{3/2}$ and $3d_{5/2}$. The binding energy of Pd 3d for each catalyst is listed in Table 3. It was found that the binding energy of all the Pd in Pd/C catalyst was shifted to the higher energy compared with pure Pd black catalyst due to the addition of carbon materials which indicates that there is a strong interaction between Pd and carbon supports.

Here, it can be said that the carbon materials really affect the performances of Pd catalysts for formic acid oxidation. From the TEM results, due to the similar particle sizes, the role of particle size effect can be excluded. Based on the previous reports, the metal-support interaction played a key role in determining the catalytic performances [34,35]. This interaction modified the electronic and catalytic properties of metal nanoparticles and led to the activation

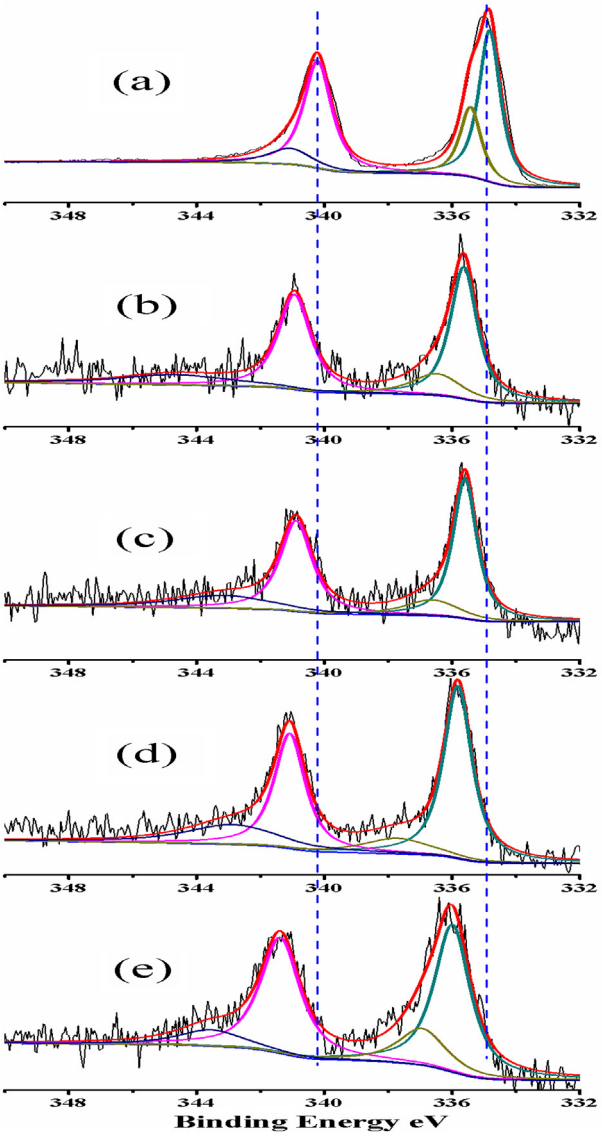


**Fig. 8.** XPS spectra of Pd 3d for Pd black (a), Pd–ACB (b), Pd–BP (c), Pd–XC (d) and Pd–MWCNT (e) catalysts.

**Table 3**
Contents of different Pd valence states from the fitting curves of Pd 3d XPS spectra.

| Catalyst samples | Binding energy of Pd (eV) | | | |
|---|---|---|---|---|
| | $3d_{5/2}$ | | $3d_{3/2}$ | |
| Valence state | (0) | (II) | (0) | (II) |
| Pd black | 334.82 | 335.43 | 340.21 | 341.13 |
| Pd–ACB | 335.65 | 336.53 | 340.94 | 344.79 |
| Pd–BP | 335.60 | 336.67 | 340.89 | 343.24 |
| Pd–XC | 335.83 | 337.77 | 341.09 | 342.95 |
| Pd–MWCNT | 336.00 | 336.99 | 341.40 | 343.65 |

of the dispersed metal for the electrode processes. The positive shift in binding energy for different carbon materials added into pure Pd black catalyst indicated a changed electronic structure and density of the state of Pd nanoparticles. Zhou et al. [36] observed that the Pd nanoparticles with higher binding energy displayed an increased activity for the formic acid electrooxidation. They attributed this observation to decreased adsorption energy of the formate intermediate, which intrinsically enhances the rate of the formic acid electrooxidation through the direct pathway. Thus, the strong interaction between the Pd and carbon promoted the formation of new active sites, which increase the activity for formic acid oxidation. Thus, we can conclude that the carbon material cannot only provide support for the noble metal nanoparticles, but possess an effect of co-catalytic/synergetic catalytic effect even though carbon material alone has almost no catalytic activity for formic acid electrooxidation.

## 4. Conclusion

The carbon material added into the pure Pd black played an important role for formic acid electrooxidation. Two formic acid oxidation peaks were observed after adding the carbon material to Pd catalyst which can be attributed to the role of the intrinsic Pd active sites and the new active sites from the Pd and C interaction. EIS confirmed that the presence of the carbon material reduced the charge transfer resistance and the resistance of intermediate oxidation, and an improved performance for fuel cell test with the carbon-modified Pd catalyst was also observed. Due to the similar particle size, the change of the performances could be attributed to the interaction between Pd and carbon as confirmed by the TEM and XPS characterization. The results are helpful in understanding the effect of carbon support in the Pd/C catalyst and reaction mechanism of formic acid electrooxidation on the Pd/C catalyst.

## Acknowledgments

The authors thank the experiential assistant of State Key Laboratory of Electroanalytical Chemistry, Laboratory of Advanced Power Sources, Changchun Institute of Applied Chemistry. This work was supported by National Basic Research Program of China (973 Program, 2012CB215500, 2012CB932800), Natural Science Foundation of Hebei Province (B2012203069), Education Department of Hebei Province on Natural Science Research Key Projects for Institution of Higher Learning (ZH2011228).

## References

[1] Y. Zhu, S.Y. Ha, R.I. Masel, J. Power Sources 130 (2004) 8–14.
[2] R. Larsen, S. Ha, J. Zakzeski, R.I. Masel, J. Power Sources 157 (2006) 78–84.
[3] J. Chang, L. Feng, C. Liu, W. Xing, X. Hu, Angew. Chem. Int. Ed. 53 (2014) 122–126.
[4] S. Ha, R. Larsen, R.I. Masel, J. Power Sources 144 (2005) 28–34.
[5] L. Zhang, Y. Tang, J. Bao, T. Lu, C. Li, J. Power Sources 162 (2006) 177–179.
[6] R.S. Jayashree, J.S. Spendelow, J. Yeom, C. Rastogi, M.A. Shannon, P.J.A. Kenis, Electrochim. Acta 50 (2005) 4674–4682.
[7] E. Antolini, Appl. Catal. B Environ. 88 (2009) 1–24.
[8] L. Feng, L. Yan, Z. Cui, C. Liu, W. Xing, J. Power Sources 196 (2011) 2469–2474.
[9] L. Feng, Z. Cui, L. Yan, W. Xing, C. Liu, Electrochim. Acta 56 (2011) 2051–2056.
[10] L. Feng, J. Yang, Y. Hu, J. Zhu, C. Liu, W. Xing, Int. J. Hydrogen Energy 37 (2012) 4812–4818.
[11] H. Tong, H.-L. Li, X.-G. Zhang, Carbon 45 (2007) 2424–2432.
[12] J. Qi, L. Jiang, Q. Tang, S. Zhu, S. Wang, B. Yi, G. Sun, Carbon 50 (2012) 2824–2831.
[13] X. Chen, G. Wu, J. Chen, Z. Xie, X. Wang, J. Am. Chem. Soc. 133 (2011) 3693–3695.
[14] S.S. Manickam, U. Karra, L. Huang, N.-N. Bui, B. Li, J.R. McCutcheon, Carbon 53 (2013) 19–28.
[15] M. Chen, Z.B. Wang, K. Zhou, Y.Y. Chu, Fuel Cells 10 (2010) 1171–1175.
[16] L. Feng, S. Yao, X. Zhao, L. Yan, C. Liu, W. Xing, J. Power Sources 197 (2012) 38–43.
[17] M. Yin, Q. Li, J.O. Jensen, Y. Huang, L.N. Cleemann, N.J. Bjerrum, W. Xing, J. Power Sources 219 (2012) 106–111.
[18] L. Feng, X. Sun, C. Liu, W. Xing, Chem. Commun. 48 (2012) 419–421.
[19] G. Zhang, Y. Wang, X. Wang, Y. Chen, Y. Zhou, Y. Tang, L. Lu, J. Bao, T. Lu, Appl. Catal. B Environ. 102 (2011) 614–619.
[20] G. Yang, Y. Chen, Y. Zhou, Y. Tang, T. Lu, Electrochem. Commun 12 (2010) 492–495.
[21] L. Li, Y. Xing, J. Electrochem. Soc. 153 (2006) A1823–A1828.
[22] Y.-R. Shin, I.-Y. Jeon, J.-B. Baek, Carbon 50 (2012) 1465–1476.
[23] K.-H. Jung, J.P. Ferraris, Carbon 50 (2012) 5309–5315.
[24] S. Siddiqui, P.U. Arumugam, H. Chen, J. Li, M. Meyyappan, ACS Nano 4 (2010) 955–961.
[25] Y. Suo, I.M. Hsing, Electrochim. Acta 55 (2009) 210–217.
[26] M. Tian, B.E. Conway, J. Electroanal. Chem. 581 (2005) 176–189.
[27] Y. Lu, W. Chen, ACS Catal. 2 (2012) 84–90.
[28] G.J. Brug, A.L.G. van den Eeden, M. Sluyters-Rehbach, J.H. Sluyters, J. Electrochem. Interface Electrochem. 176 (1984) 275–295.
[29] G.J. Brug, M. Sluyters-Rehbach, J.H. Sluyters, A. Hemelin, J. Electrochem. Interface. Electrochem. 181 (1984) 245–266.
[30] B. Hirschorn, M.E. Orazem, B. Tribollet, V. Vivier, I. Frateur, M. Musiani, Electrochim. Acta 55 (2010) 6218–6227.
[31] Z. Lukács, J. Electroanal. Chem. 464 (1999) 68–75.
[32] Z. Lukfics, J. Electroanal. Chem. 432 (1997) 79–83.
[33] R.L. Hurt, J.R. Macdonald, Solid State Ionics 20 (1986) 111–124.
[34] X. Zhao, J. Zhu, L. Liang, C. Li, C. Liu, W. Xing, Appl. Catal. B Environ. 129 (2013) 146–152.
[35] J. Chang, X. Sun, L. Feng, W. Xing, X. Qin, G. Shao, J. Power Sources 239 (2013) 94–102.
[36] W.P. Zhou, A. Lewera, R. Larsen, R.I. Masel, P.S. Bagus, A. Wieckowski, J. Phys. Chem. B 110 (2006) 13393–13398.